Type-II Dirac semimetals in the YPd_2Sn class

Peng-Jie Guo, Huan-Cheng Yang, Kai Liu,* and Zhong-Yi Lu†
Department of Physics and Beijing Key Laboratory of Opto-electronic Functional Materials & Micro-nano Devices, Renmin University of China, Beijing 100872, China
(Received 22 December 2016; revised manuscript received 21 February 2017; published 10 April 2017)

Lorentz-invariance-violating Weyl and Dirac fermions have recently attracted intensive interests as new types of particles beyond high-energy physics, and they demonstrate novel physical phenomena such as angle-dependent chiral anomaly and topological Lifshitz transitions. Here, we predict the existence of Lorentz-invariance-violating Dirac fermions in the YPd_2Sn class of Heusler alloys that emerge at the boundary between the electronlike and holelike pockets in the Brillouin zone, based on first-principles electronic structure calculations. In combination with the fact that this class of materials was reported to be superconductors, the YPd_2Sn class provides an appropriate platform for studying exotic physical properties distinguished from conventional Dirac fermions, especially for realizing possible topological superconductivity.

DOI: 10.1103/PhysRevB.95.155112

I. INTRODUCTION

Conceptually, by generalizing the topological characterization from insulator to metal, it has been realized that the Dirac [1–4] and Weyl semimetals [5–9] are new classes of three-dimensional (3D) topological materials, different from the well-studied 3D topological insulators (TIs) [10–13]. For Dirac semimetals with both time-reversal and space-inversion symmetries, a Dirac point is a linear crossing of two doubly degenerate bands near the Fermi energy with its stability protected by additional symmetry, such as a certain crystalline symmetry, while a Weyl point can be obtained by breaking either time-reversal or space-inversion symmetry in Dirac semimetals, which is a linear crossing of two nondegenerate bands near the Fermi energy only available in 3D. A Weyl point acts as a magnetic monopole with either positive or negative charge (chirality) in 3D momentum space, while a Dirac point represents a pair of magnetic monopoles with opposite charges. Thus, Dirac and Weyl semimetals possess a large variety of novel phenomena, such as quantum magnetoresistance [14] and chiral anomaly [15]. In addition, Dirac and Weyl fermions in condensed matter physics correspond to relativistic Dirac and Weyl fermions in high-energy physics. Nevertheless, the Lorentz invariance is only strictly required in high-energy physics but not necessary in condensed matter physics [16]. This brings hope for condensed matter physicists to discover new types of fermions in real materials.

Very recently, Lorentz-invariance-violating, namely, type-II, Weyl and Dirac fermions were first conceptually proposed and further predicted in several compounds [16–22], in whose energy spectra a Dirac cone is strongly tilted to a certain direction by a linear kinetic component to break the Lorentz invariance. Experimentally, the compounds WTe_2 and $MoTe_2$ have been confirmed to host type-II Weyl fermions [23–30], while type-II Dirac fermions have been verified in $PtTe_2$ by angle-resolved photoemission spectroscopy (ARPES) measurements [31]. Different from conventional (type-I) Weyl or Dirac fermions, type-II Weyl or Dirac fermions are located at the boundary between the electronlike and holelike pockets in the Brillouin zone, expectedly showing many unusual physical properties, such as angle-dependent chiral anomaly [16,32,33] and topological Lifshitz transitions [16,22].

In comparison with type-II Weyl semimetals [23–30], type-II Dirac semimetals, which are proposed as improved platforms to afford topological superconductivity and to explore Majorana fermions [34], are much less studied. Up to now, there have been only three classes of type-II Dirac semimetals reported: RbMgBi [20], VAl_3 [21], and $PtSe_2$ classes [22], respectively. The former two have still only been predicted theoretically. For the last one, the Dirac points have been experimentally verified but relatively far from the Fermi level [31]. Moreover, due to their tetragonal or hexagonal crystal structures, these three classes of compounds possess just one pair of Dirac points along the k_z direction in the bulk Brillouin zone. It is thus very important and urgent to search for new type-II Dirac semimetal materials with more pairs of Dirac points sufficiently close to the Fermi level and playing an important role.

The Heusler alloys in real materials are a very large family with abundant physical properties [35]. Dozens of TIs were theoretically predicted in half Heusler alloys [36–40]. Among them, some half Heusler alloys are possibly antiferromagnetic topological insulators (AFTIs) [41–43], while some other half Heusler TIs show superconducting behavior [44–47] and may realize topological superconductivity [48,49]. Although intensive attention has been paid on half Heusler alloys, the likely topological electronic states of full Heusler alloys are rarely studied [50,51].

Here, we predict the existence of type-II Dirac fermions in the full Heusler alloys YPd_2Sn, $ScPd_2Sn$, $ZrPd_2Al$, $HfPd_2Al$, $ZrNi_2Al$, and $HfNi_2Al$, namely, the YPd_2Sn class, by using first-principles electronic structure calculations. For this class, we find that there are three pairs of symmetry-protected type-II Dirac fermions located respectively along three equivalent Γ-X paths in the bulk Brillouin zone.

II. COMPUTATIONAL DETAILS

First-principles electronic structure calculations were performed with the projector augmented wave (PAW) method [52]

*kliu@ruc.edu.cn
†zlu@ruc.edu.cn

as implemented in the Vienna *ab initio* simulation package (VASP) [53]. The generalized gradient approximation (GGA) of Perdew-Burke-Ernzerhof (PBE) type was adopted for the exchange-correlation potential. The kinetic energy cutoff of the plane wave basis was set to be 340 eV. A $10 \times 10 \times 10$ **k**-point mesh for the Brillouin zone (BZ) sampling and a Gaussian smearing with a width of 0.05 eV around the Fermi surface were adopted. Both cell parameters and internal atomic positions were fully relaxed until the forces on all atoms were smaller than 0.01 eV/Å. The maximally localized Wannier function (MLWF) [54,55] method was used to calculate the Fermi surface. To study the topological surface states, a 1×1 two-dimensional supercell with an AB_2C slab containing 66 atoms and a 15 Å vacuum was employed to simulate the AB_2C (001) surface.

III. RESULTS AND ANALYSIS

The crystal structure of the full Heusler alloys AB_2C takes the $Fm\bar{3}m$ space group symmetry [Fig. 1(a)]. The elements

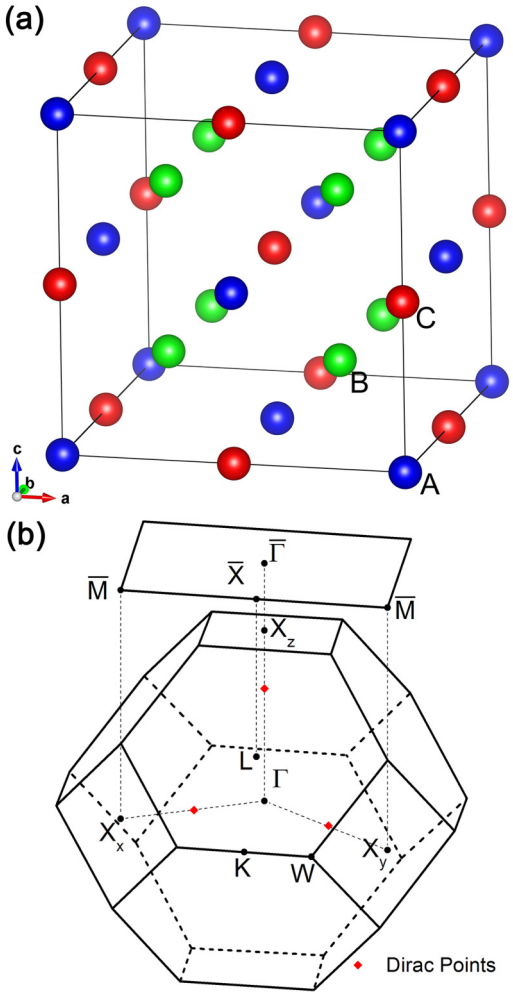

FIG. 1. (a) Crystal structure of the full Heusler alloys AB_2C with $Fm\bar{3}m$ symmetry. (b) Bulk Brillouin zone and the projected surface Brillouin zone of an AB_2C (001) surface. The black dots represent the high-symmetry **k** points in the Brillouin zone while the red ones denote the Dirac points.

TABLE I. Calculated and experimental (in parentheses) lattice constants a (in units of Å) of several full Heusler alloys. The locations of the Dirac points along the Γ-X directions in the BZ (k_x) and their energies (E_D) with respect to the Fermi level. The superconducting transition temperatures T_c's reported in the literature.

	a (Å)	k_x (π/a)	E_D (meV)	T_c (K)
$ZrNi_2Al$	6.122(6.106)[a]	0.381	−296	1.38[a]
$HfNi_2Al$	6.088(6.069)[a]	0.361	−257	0.74[a]
$ZrPd_2Al$	6.451(6.390)[b]	0.363	−270	3.2[b]
$HfPd_2Al$	6.417(6.370)[b]	0.348	−232	3.4[b]
$ScPd_2Sn$	6.580(6.509)[c]	0.239	142	2.25[c]
YPd_2Sn	6.787(6.718)[a]	0.223	129	4.9[a]

[a]Reference [56].
[b]Reference [57].
[c]Reference [58].

A and C make up the rocksalt structure, and the element B is located at the $(\frac{1}{4},\frac{1}{4},\frac{1}{4})$ coordinate and its equivalent positions. As listed in Table I, the fully relaxed lattice constants of the Heusler alloys from our calculations accord well with their corresponding experimental values [56–58]. In the bulk BZ of the Heusler alloys we studied [Fig. 1(b)], the black dots represent the high-symmetry **k** points, while the red dots schematically display the locations of Dirac points along the Γ-X directions.

We first show the electronic band structure of YPd_2Sn as a representative case of the Dirac semimetals in the full Heusler alloys we predict (Fig. 2). Without spin-orbital coupling (SOC), a band crossing close to the Fermi level along the Γ-X direction can be clearly observed [Fig. 2(a)]. Once the SOC is included in the calculations, two doubly degenerate bands along the Γ-L and Γ-X directions split [Fig. 2(b)]. Nevertheless, the above band crossing along the Γ-X direction still holds, with only a minor energy shift. As these two bands are both doubly degenerate bands due to the time-reversal and space-inversion symmetries in YPd_2Sn, this crossing point is fourfold degenerate. We thus suggest that this band crossing point is a Dirac point protected by the C_{4v} double group in YPd_2Sn. To prove it, we have calculated the parities for the bands around the Fermi level at the high-symmetry points Γ and X and analyzed the orbital characteristics of these two crossing bands.

As there are three equivalent X points in the BZ for the cubic symmetry [Fig. 1(b)], we have studied the orbital information of the crossing bands along three different Γ-X directions. By analyzing all orbitals (s, p, and d) of the Y, Pd, and Sn atoms, we find that the two crossing bands (α and β) mainly consist of the $4d$ orbitals of the Y atom, the $5s$ and $5p$ orbitals of the Sn atom, and the $4d$ orbitals of two centrosymmetric Pd atoms (Fig. 3). Among them, the $5s$ orbital of the Sn atom makes an isotropic contribution to the two crossing bands along three different Γ-X directions. In contrast, the contributions from the $5p$ and $4d$ orbitals are anisotropic.

For the α band, the orbital characteristics change gradually from the Sn s orbital at the Γ point to the Sn p orbital [Fig. 3(a)] as well as the d orbitals of two centrosymmetric Pd atoms toward the X point [Fig. 3(b)]. By analyzing the parity and the orbital characteristics, the symmetries are Γ_6^+ at the Γ point, Δ_6

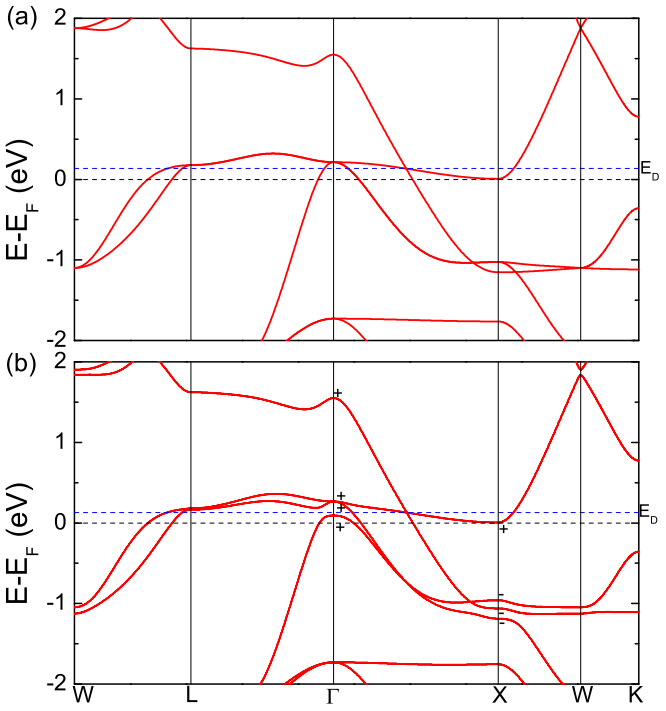

FIG. 2. Band structures along the high-symmetry directions of the Brillouin zone for YPd_2Sn calculated (a) without and (b) with the spin-orbital-coupling (SOC) effect. The Fermi level is set to zero. The E_D denotes the energy of the Dirac point. The signs "+" and "−" indicate the parities of the corresponding states at the high-symmetry points Γ and X.

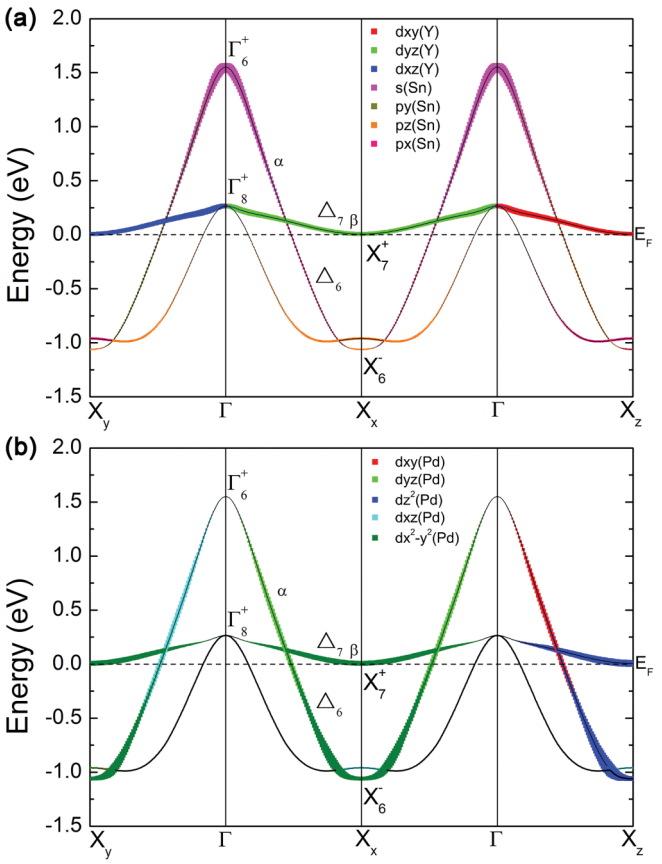

FIG. 3. Orbital characteristics of the two crossing bands α and β contributed from different orbitals of (a) Y/Sn and (b) Pd atoms and their symmetries along the Γ-X directions. The Fermi level is set to zero. The signs "+" and "−" indicate the parities of corresponding states.

along the Γ-X axis, and X_6^- at the X point, respectively [59]. On the other hand, for the β band, the contributions change from Y t_{2g} orbitals at the Γ point to both the t_{2g} orbitals of the Y atom and the e_g orbitals of two centrosymmetric Pd atoms toward the X point. The respective symmetries are Γ_8^+, Δ_7, and X_7^+ at the Γ point, along the Γ-X direction, and at the X point [59]. Here, Δ_6 and Δ_7 are respectively two inequivalent irreducible representations of the C_{4v} double group in YPd_2Sn, therefore these crossing points of the α and β bands in the Γ-X directions are protected by the symmetry of the C_{4v} double group.

More importantly, the Dirac cone is tilted strongly along the Γ-X axis, which is a typical feature of type-II Dirac fermions. According to our calculations on YPd_2Sn, there are three pairs of symmetry-protected Dirac points, which are located at $k = (0,0,\pm 0.223)$, $(0,\pm 0.223,0)$, and $(\pm 0.223,0,0)$ (in units of π/a) on the equivalent Γ-X axes with an energy of $E_D = 129$ meV above the Fermi level. Remarkably, the electronic band structures of other YPd_2Sn class materials ($ZrNi_2Al$, $HfNi_2Al$, $ZrPd_2Al$, $HfPd_2Al$, and $ScPd_2Sn$) are very similar (see the Appendix). All of them show features of type-II Dirac semimetals. The respective positions of the Dirac points for this class of materials are summarized in Table I. Among them, the Dirac cone of YPd_2Sn is the most tilted and its E_D is the closest to the Fermi level.

Based on the above parity, orbital-characteristic, and group-theory analysis of the crossing bands α and β, we clarify that type-II Dirac points exist in the electronic band structure of YPd_2Sn. For type-I Dirac semimetals such as Na_3Bi and Cd_3As_2 [3,4], the Fermi surface becomes a number of points when the Fermi level is located at the Dirac-point energy (E_D). In contrast, for a type-II Dirac semimetal, a part of the upper Dirac cone is lower than a part of the lower cone, thus retaining both electronlike and holelike pockets touching each other when the Fermi level crosses E_D. This is exactly the case for YPd_2Sn as shown in Fig. 4(b). When the Fermi level is lower than E_D, the electronlike pockets become smaller

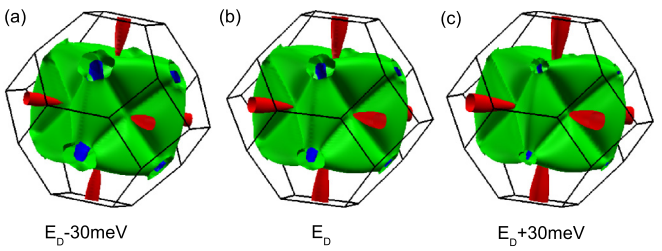

FIG. 4. The isoenergetic surfaces of YPd_2Sn at (a) $E_D - 30$ meV, (b) E_D, and (c) $E_D + 30$ meV in bulk BZ. The red surfaces are electronlike pockets while the green and blue surfaces are holelike pockets. Contact between the electronlike and holelike pockets occurs at the Dirac points when $E = E_D$.

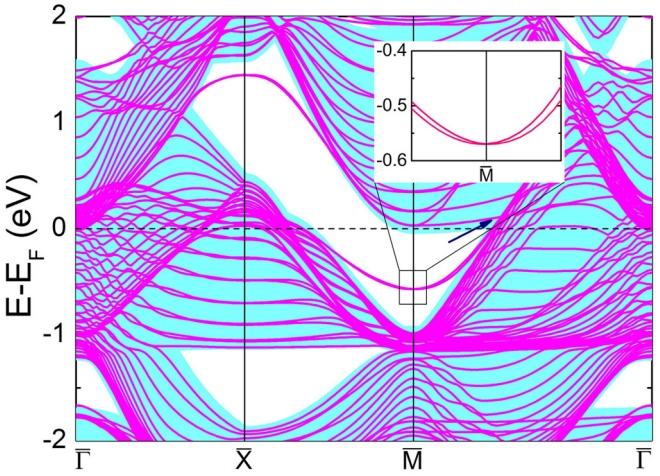

FIG. 5. Surface band structure of the YSn-terminated YPd_2Sn (001) surface along the high-symmetry directions of the surface Brillouin zone [Fig. 1(b)]. The inset shows the enlarged region for the surface states around $\overline{M}$, while the arrow points to the zone where the surface bands merge with the bulk continuum. The shaded cyan areas denote the surface-projected bulk states.

while the holelike pockets become larger [Fig. 4(a)], and vice versa [Fig. 4(c)]. Once the Fermi level deviates from the Dirac point, the electronlike pockets and holelike pockets will separate from each other (Figs. 4 and 2). Therefore, a Lifshitz transition of the Fermi surfaces can be observed in type-II Dirac semimetals by tuning the Fermi level.

Symmetry-protected topological surface states are one of the most important phenomena for Dirac semimetals. We thus have calculated the surface states of YPd_2Sn (Fig. 5). For the YPd_2Sn (001) surface, two Dirac points along the Γ-X_z direction in the bulk BZ are projected to the $\overline{\Gamma}$ point in the surface BZ and the other four Dirac points are projected to the $\overline{\Gamma}$-$\overline{M}$ directions of the surface BZ [Fig. 1(b)]. As shown in Fig. 5, two surface states below the Fermi level around $\overline{M}$ merge into the bulk continuum at the projected bulk Dirac point along the $\overline{\Gamma}$-$\overline{M}$ direction (marked by the blue arrow). These are the symmetry-protected topological surface states [20]. The other surface states, for instance, the surface states above the Fermi level at $\overline{X}$ in the surface BZ, do not conflate with the bulk continuum at the bulk Dirac point. We thus deduce that the other surface states are normal surface states.

IV. DISCUSSION

The type-II Dirac semimetals predicted in this study have many advantages. First, due to the $Fm\bar{3}m$ symmetry of their face-centered-cubic (fcc) primitive cells (Fig. 1), there are more Dirac-point pairs in the bulk BZ of the YPd_2Sn class than those of the hexagonal $PtSe_2$ class as well as the tetragonal RbMgBi and VAl_3 families. These Dirac points remain after surface projection and their corresponding topological surface states are prone to be detected in ARPES measurements. Second, the Dirac points of the YPd_2Sn class are all close to the Fermi level (Table I). Especially, the Dirac-point energy of YPd_2Sn is just 129 meV above the Fermi level, which reduces to 75 meV when the lattice constants are compressed by 3%. By tuning the Fermi level with a gate voltage, an angle-dependent chiral anomaly may be observed in transport experiments. Lastly, in different YPd_2Sn class materials, the Dirac points are located either above or below the Fermi level (Table I). Thus, by proper element substitution or lattice modulation, the energy of a Dirac point may well be located on the Fermi level.

Another striking point is that the entire YPd_2Sn class of compounds was reported to be superconductors in previous experiments (Table I). As suggested by a recent study [34], compared with Weyl semimetals and conventional Dirac semimetals, a wealth of density of states provided by the electronlike and holelike pockets near the Dirac points in type-II Dirac semimetals is beneficial to the carrier ratio of a possible topological superconductor. Thus, the YPd_2Sn class may serve as prototypical systems to study topological superconductivity and to search for Majorana fermions, which have potential applications in quantum computation. Furthermore, from a crystal-structure standpoint, the YPd_2Sn class belongs to naturally abundant Heusler compounds with versatile nonmagnetic, magnetic, semiconducting, metallic, superconducting, and topological properties [35]. We expect that full (half) Heusler compounds will provide many chances to discover new topological semimetals and possible topological superconductors.

V. SUMMARY

By using first-principles electronic structure calculations, we predict the existence of type-II Dirac fermions that are located at the boundary between the electronlike and holelike

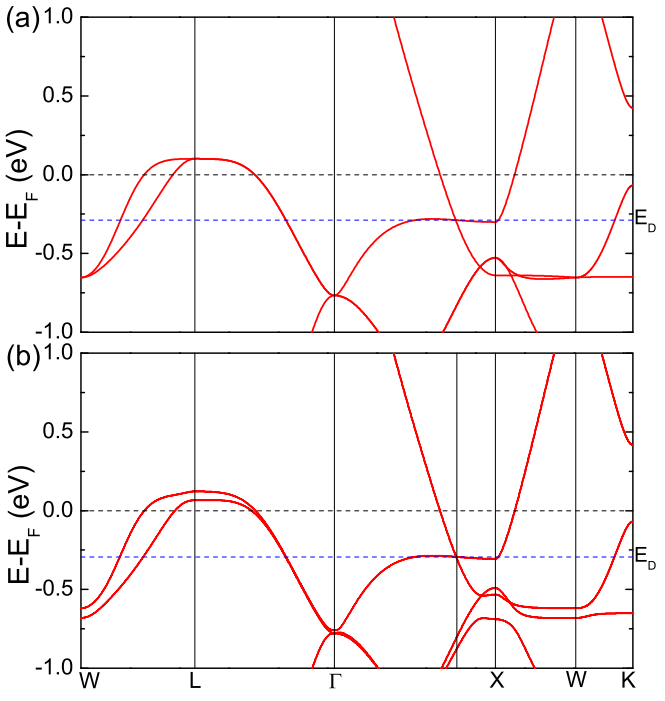

FIG. 6. Band structures along the high-symmetry directions of the Brillouin zone for $ZrNi_2Al$ calculated (a) without and (b) with the spin-orbital-coupling (SOC) effect. The Fermi level is set to zero. The E_D denotes the energy of the Dirac point.

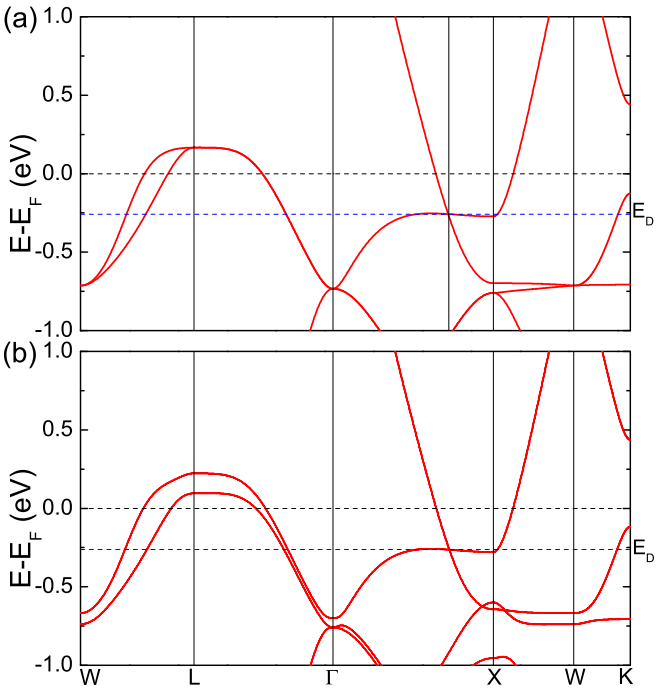

FIG. 7. Band structures along the high-symmetry directions of the Brillouin zone for $HfNi_2Al$ calculated (a) without and (b) with the spin-orbital-coupling (SOC) effect. The Fermi level is set to zero. The E_D denotes the energy of the Dirac point.

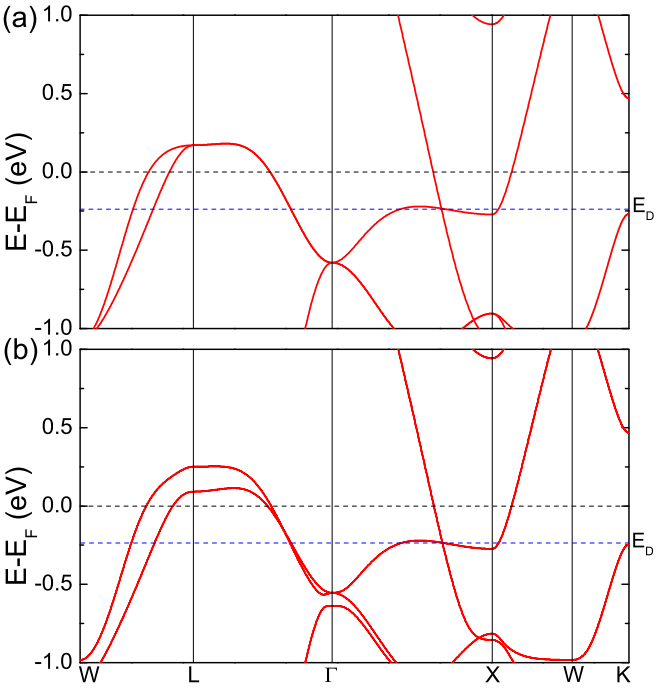

FIG. 9. Band structures along the high-symmetry directions of the Brillouin zone for $HfPd_2Al$ calculated (a) without and (b) with the spin-orbital-coupling (SOC) effect. The Fermi level is set to zero. The E_D denotes the energy of the Dirac point.

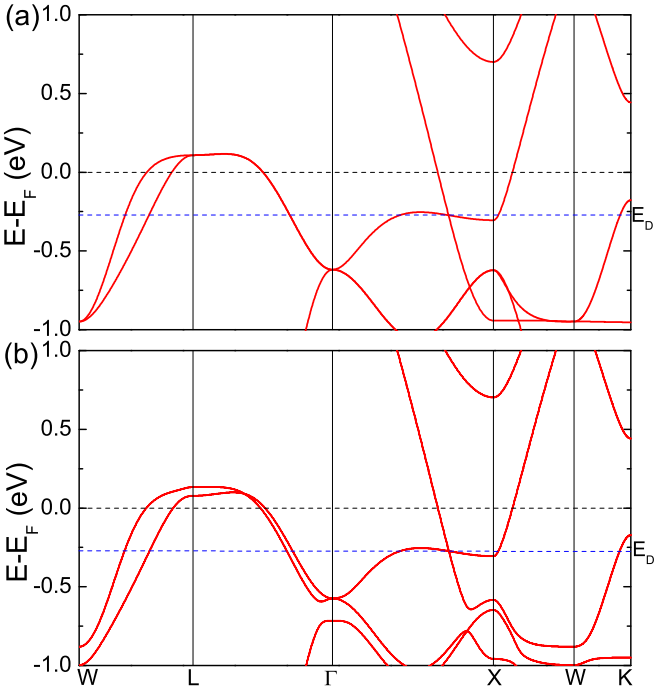

FIG. 8. Band structures along the high-symmetry directions of the Brillouin zone for $ZrPd_2Al$ calculated (a) without and (b) with the spin-orbital-coupling (SOC) effect. The Fermi level is set to zero. The E_D denotes the energy of the Dirac point.

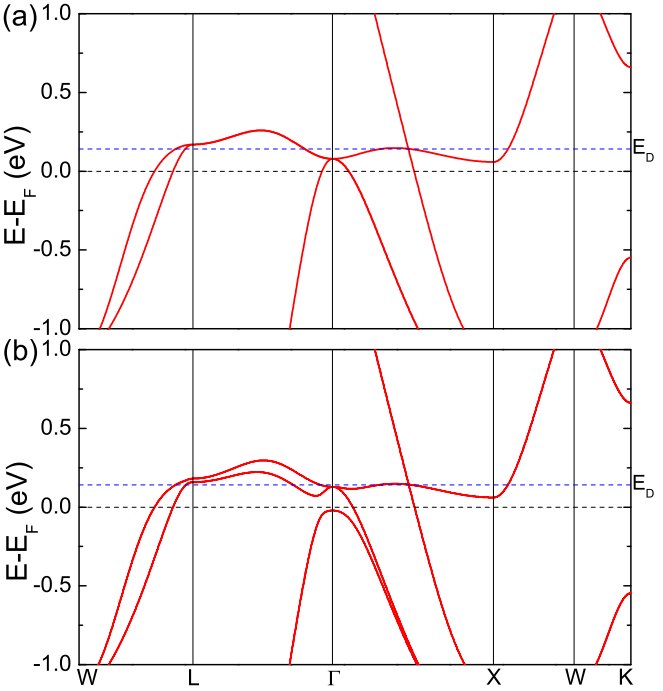

FIG. 10. Band structures along the high-symmetry directions of the Brillouin zone for $ScPd_2Sn$ calculated (a) without and (b) with the spin-orbital-coupling (SOC) effect. The Fermi level is set to zero. The E_D denotes the energy of the Dirac point.

pockets in the YPd_2Sn class. Benefiting from the symmetry of their fcc crystal structures, three pairs of type-II Dirac points appear on the Γ-X directions of the bulk BZ. Considering that these compounds were all reported to be superconductors, the YPd_2Sn class provides a platform to study exotic physical properties distinguished from conventional Dirac fermions and to realize possible topological superconductivity.

ACKNOWLEDGMENTS

We thank Yuan-Yao He, Xin-Zheng Li, Zheng-Xin Liu, Ning-Hua Tong, Rui Lou, and Tao Li for helpful conversations. This work was supported by the National Natural Science Foundation of China (Grants No. 11474356 and No. 91421304), the Fundamental Research Funds for the Central Universities, and the Research Funds of Renmin University of China (Grants No. 14XNLQ03 and No. 16XNLQ01). Computational resources have been provided by the Physical Laboratory of High Performance Computing at Renmin University of China. The Fermi surfaces were prepared with the XCRYSDEN program [60].

APPENDIX: BAND STRUCTURES OF OTHER TYPE-II DIRAC SEMIMETALS IN THE YPd_2Sn CLASS

Here, we provide the calculated electronic band structures of other YPd_2Sn-class materials, i.e., $ZrNi_2Al$, $HfNi_2Al$, $ZrPd_2Al$, $HfPd_2Al$, and $ScPd_2Sn$, along the high-symmetry directions of the bulk Brillouin zone in Figs. 6–10, respectively.

[1] S. M. Young, S. Zaheer, J. C. Y. Teo, C. L. Kane, E. J. Mele, and A. M. Rappe, Phys. Rev. Lett. **108**, 140405 (2012).
[2] J. L. Mañes, Phys. Rev. B **85**, 155118 (2012).
[3] Z. J. Wang, Y. Sun, X. Q. Chen, C. Franchini, G. Xu, H. M. Weng, X. Dai, and Z. Fang, Phys. Rev. B **85**, 195320 (2012).
[4] Z. J. Wang, H. M. Weng, Q. Wu, X. Dai, and Z. Fang, Phys. Rev. B **88**, 125427 (2013).
[5] X. G. Wan, A. M. Turner, A. Vishwanath, and S. Y. Savrasov, Phys. Rev. B **83**, 205101 (2011).
[6] G. Xu, H. M. Weng, Z. J. Wang, X. Dai, and Z. Fang, Phys. Rev. Lett. **107**, 186806 (2011).
[7] A. A. Burkov and L. Balents, Phys. Rev. Lett. **107**, 127205 (2011).
[8] A. A. Burkov, M. D. Hook, and L. Balents, Phys. Rev. B **84**, 235126 (2011).
[9] G. B. Halász and L. Balents, Phys. Rev. B **85**, 035103 (2012).
[10] H. J. Zhang, C. X. Liu, X. L. Qi, X. Dai, Z. Fang, and S. C. Zhang, Nat. Phys. **5**, 438 (2009).
[11] Y. Dai, D. Qian, D. Hsieh, L. Wray, A. Pal, H. Lin, A. Bansil, D. Grauer, Y. S. Hor, R. J. Cava, and M. Z. Hasan, Nat. Phys. **5**, 398 (2009).
[12] Y. L. Chen, J. G. Analytis, J. H. Chu, Z. K. Liu, S. K. Mo, X. L. Qi, H. J. Zhang, X. Dai, Z. Fang, S. C. Zhang *et al.*, Science **325**, 178 (2009).
[13] M. Z. Hasan and C. L. Kane, Rev. Mod. Phys. **82**, 3045 (2010); X.-L. Qi and S.-C. Zhang, *ibid.* **83**, 1057 (2011).
[14] A. A. Abrikosov, Phys. Rev. B **58**, 2788 (1998).
[15] H. B. Nielsen and M. Ninomiya, Phys. Lett. B **130**, 389 (1983).
[16] A. A. Soluyanov, D. Gresch, Z. Wang, Q. Wu, M. Troyer, X. Dai, and B. A. Bernevig, Nature (London) **527**, 495 (2015).
[17] Y. Sun, S.-C. Wu, M. N. Ali, C. Felser, and B.-H. Yan, Phys. Rev. B **92**, 161107(R) (2015).
[18] T. R. Chang, S. Y. Xu, G. Q. Chang, C. C. Lee, S. M. Huang, B. K. Wang, G. Bian, H. Zheng, D. S. Sanchez, I. Belopolski *et al.*, Nat. Commun. **7**, 10639 (2016).
[19] Z. Wang, D. Gresch, A. A. Soluyanov, W. W. Xie, S. Kushwaha, X. Dai, M. Troyer, R. J. Cava, and B. A. Bernevig, Phys. Rev. Lett. **117**, 056805 (2016).
[20] C.-C. Le, S.-S. Qin, X.-X. Wu, X. Dai, P.-Y. Fu, and J.-P. Hu, arXiv:1606.05042.
[21] T.-R. Chang, S. Y. Xu, D. S. Sanchez, S. M. Huang, G. Q. Chang, C.-H. Hsu, G. Bian, I. Belopolski, Z.-M. Yu, X. C. Xu *et al.*, arXiv:1606.07555.
[22] H. Q. Huang, S. Y. Zhou, and W. H. Duan, Phys. Rev. B **94**, 121117(R) (2016).
[23] K. Deng, G. Wan, P. D. K. Zhang, S. J. Ding, E. Y. Wang, M. Z. Yan, H. Q. Huang, H. Y. Zhang, Z. L. Xu, J. Denlinger *et al.*, Nat. Phys. **12**, 1105 (2016).
[24] L. N. Huang, T. M. McCormick, M. Ochi, Z. Y. Zhao, M. T. Suzuki, R. Arita, Y. Wu, D.-X. Mou, H.-B. Cao, J. Q. Yan *et al.*, Nat. Mater. **15**, 1155 (2016).
[25] N. Xu, Z. J. Wang, A. P. Weber, A. Magrez, P. Bugnon, H. Berger, C. E. Matt, J. Z. Ma, B. B. Fu, B. Q. Lv *et al.*, arXiv:1604.02116.
[26] A. J. Liang, J. W. Huang, S. M. Nie, Y. Ding, Q. Gao, C. Hu, S. L. He, Y. X. Zhang, C. L. Wang, B. Shen *et al.*, arXiv:1604.01706.
[27] J. Jiang, Z. K. Liu, Y. Sun, H. F. Yang, R. Rajamathi, Y. P. Qi, L. X. Yang, C. Chen, H. Peng, C.-C. Hwang *et al.*, Nat. Commun. **8**, 13973 (2017).
[28] F. Y. Bruno, A. Tamai, Q. S. Wu, I. Cucchi, C. Barreteau, A. de la Torre, S. McKeown Walker, S. Riccò, Z. Wang, T. K. Kim *et al.*, Phys. Rev. B **94**, 121112(R) (2016).
[29] Y. Wu, D. X. Mou, N. H. Jo, K. W. Sun, L. N. Huang, S. L. Bud'ko, P. C. Canfield, and A. Kaminski, Phys. Rev. B **94**, 121113(R) (2016).
[30] C. L. Wang, Y. Zhang, J. W. Huang, S. M. Nie, G. D. Liu, A. J. Liang, Y. X. Zhang, B. Shen, J. Liu, C. Hu *et al.*, Phys. Rev. B **94**, 241119 (2016).
[31] M. Z. Yan, H. Q. Huang, K. N. Zhang, E. Y. Wang, W. Yao, K. Deng, G. L. Wan, H. Y. Zhang, M. Arita, H. T. Yang *et al.*, arXiv:1607.03643.
[32] K. Zhang and G. E. Volovik, arXiv:1604.00849.
[33] Y. Xu, F. Zhang, and C. Zhang, Phys. Rev. Lett. **115**, 265304 (2015).
[34] F. C. Fei, X. Y. Bo, R. Wang, B. Wu, J. Jiang, D. Z. Fu, M. Gao, H. Zheng, Y. L. Chen, F. Q. Song *et al.*, arXiv:1611.08112.
[35] T. Graf, C. Felser, and S. S. P. Parkin, Prog. Solid State Chem. **39**, 1 (2011).
[36] S. Chadov, X. L. Qi, J. Kubler, G. H. Fecher, C. Felser, and S. C. Zhang, Nat. Mater. **9**, 541 (2010).
[37] H. Lin, L. A. Wray, Y. Q. Xia, S. Y. Xu, S. Jia, R. J. Cava, A. Bansil, and M. Z. Hasan, Nat. Mater. **9**, 546 (2010).

[38] D. Xiao, Y. G. Yao, W. X. Feng, J. Wen, W. G. Zhu, X.-Q. Chen, G. M. Stocks, and Z. Y. Zhang, Phys. Rev. Lett. **105**, 096404 (2010).
[39] W. Al-Sawai, H. Lin, R. S. Markiewicz, L. A. Wray, Y. Xia, S.-Y. Xu, M. Z. Hasan, and A. Bansil, Phys. Rev. B **82**, 125208 (2010).
[40] W. X. Feng, D. Xiao, Y. Zhang, and Y. G. Yao, Phys. Rev. B **82**, 235121 (2010).
[41] R. S. K. Mong, A. M. Essin, and J. E. Moore, Phys. Rev. B **81**, 245209 (2010).
[42] R. A. Müller, N. R. Lee-Hone, L. Lapointe, D. H. Ryan, T. Pereg-Barnea, A. D. Bianchi, Y. Mozharivskyj, and R. Flacau, Phys. Rev. B **90**, 041109(R) (2014).
[43] R. A. Müller, A. Desilets-Benoit, N. Gauthier, L. Lapointe, A. D. Bianchi, T. Maris, R. Zahn, R. Beyer, E. Green, J. Wosnitza, Z. Yamani, and M. Kenzelmann, Phys. Rev. B **92**, 184432 (2015).
[44] N. P. Butch, P. Syers, K. Kirshenbaum, A. P. Hope, and J. Paglione, Phys. Rev. B **84**, 220504(R) (2011).
[45] F. F. Tafti, T. Fujii, A. Juneau-Fecteau, S. René de Cotret, N. Doiron-Leyraud, A. Asamitsu, and L. Taillefer, Phys. Rev. B **87**, 184504 (2013).
[46] G. Z. Xu, W. H. Wang, X. M. Zhang, Y. Du, E. K. Liu, S. G. Wang, G. H. Wu, Z. Y. Liu, and X. X. Zhang, Sci. Rep. **4**, 5709 (2014).
[47] M. Meinert, Phys. Rev. Lett. **116**, 137001 (2016).
[48] C.-K. Chiu, P. Ghaemi, and T. L. Hughes, Phys. Rev. Lett. **109**, 237009 (2012).
[49] C. Fang, B. A. Bernevig, and M. J. Gilbert, Phys. Rev. B **91**, 165421 (2015).
[50] C. Li, J. S. Lian, and Q. Jiang, Phys. Rev. B **83**, 235125 (2011).
[51] X.-T. Wang, X.-F. Dai, H.-Y. Jia, L.-Y. Wang, R. Liu, Y. Li, X.-C. Liu, X.-M. Zhang, W.-H. Wang, G.-H. Wu, and G.-D. Liu, Acta Phys. Sin. **63**, 23101 (2014).
[52] P. E. Blöchl, Phys. Rev. B **50**, 17953 (1994); G. Kresse and D. Joubert, *ibid.* **59**, 1758 (1999).
[53] G. Kresse and J. Hafner, Phys. Rev. B **47**, 558 (1993); G. Kresse and J. Furthmüller, Comput. Mater. Sci. **6**, 15 (1996); Phys. Rev. B **54**, 11169 (1996).
[54] N. Marzari and D. Vanderbilt, Phys. Rev. B **56**, 12847 (1997).
[55] I. Souza, N. Marzari, and D. Vanderbilt, Phys. Rev. B **65**, 035109 (2001).
[56] J. H. Wernick, G. W. Hull, T. H. Geballe, J. E. Bernardini, and J. V. Waszczak, Mater. Lett. **2**, 90 (1983).
[57] J. Winterlik, G. H. Fecher, and C. Felser, Solid State Commun. **145**, 475 (2008).
[58] M. J. Johnson and R. N. Shelton, Solid State Commun. **52**, 839 (1984).
[59] G. F. Koster, J. O. Dimmock, R. G. Wheeler, and H. Statz, *Properties of the Thirty-Two Point Groups* (MIT Press, Cambridge, MA, 1963).
[60] A. Kokalj, Comput. Mater. Sci. **28**, 155 (2003).